PROCEEDINGS OF SPIE

SPIEDigitalLibrary.org/conference-proceedings-of-spie

Elucidating the neuropathophysiology of COVID-19 using quantum dot biomimetics of SARS-CoV-2

Chiang, Wesley, Urban, Jennifer, Litzburg, Angela, Nilsson, Bradley, Gelbard, Harris, et al.

Wesley Chiang, Jennifer Urban, Angela Litzburg, Bradley Nilsson, Harris Gelbard, Todd Krauss, "Elucidating the neuropathophysiology of COVID-19 using quantum dot biomimetics of SARS-CoV-2," Proc. SPIE 11977, Colloidal Nanoparticles for Biomedical Applications XVII, 1197702 (3 March 2022); doi: 10.1117/12.2609118

Event: SPIE BiOS, 2022, San Francisco, California, United States

Downloaded From: https://www.spiedigitallibrary.org/conference-proceedings-of-spie on 17 Apr 2022 Terms of Use: https://www.spiedigitallibrary.org/terms-of-use

Elucidating the neuropathophysiology of COVID-19 using quantum dot biomimetics of SARS-CoV-2

Wesley Chiang*[a], Jennifer Urban[b], Angela Litzburg[c], Bradley Nilsson[b], Harris Gelbard[c,d], Todd Krauss[b,e]

[a]Dept. of Biochemistry and Biophysics; [c]Center for Neurotherapeutic Discovery and Dept. of Neurology; [d]Depts. of Pediatrics, Neuroscience, and Microbiology and Immunology, University of Rochester Medical Center, Rochester, NY USA 14642
[b]Dept. of Chemistry; [e]The Institute of Optics, University of Rochester, Rochester, NY USA 14627

ABSTRACT

Quantum dots were encapsulated in polymeric phospholipid micelles conjugated to multiple ligands of SARS-CoV-2 spike protein to form fluorescent biomimetic nanoparticles for SARS-CoV-2 (COVID-QDs). Phosphatidylethanolamine-polyethylene glycol (PE:PEG) was appended with bis(4-methylphenyl)sulfone to form PE:PEG:bis-sulfone and self-assembled into micelles around CdSe/CdS core/shell quantum dots via thin-film rehydration. The introduction of the bis-sulfone group the surface of the micelle-encapsulated quantum dots provides multiple sites for conjugation to his-tagged SARS-CoV-2 spike protein via a bisalkylation mechanism. Based on the eluted unconjugated fraction, we estimate that an average of seven spike proteins are conjugated per COVID-QD. We treated an in-vitro model system for the neurovascular unit (NVU) with these COVID-QD constructs to investigate the COVID-QDs, and by proxy SARS-CoV-2, may modulate the NVU leading to the COVID-19 associated neuropathophysiology.

Keywords: Biomimetic Nanoparticles, Quantum Dots, SARS-CoV-2, Neuro-COVID, Neuroimmunology, blood-brain barrier

1. INTRODUCTION

Compared to traditional fluorophores, colloidal semiconductor quantum dots (QDs) exhibit enhanced photophysical properties that are of interest to biological applications, not limited to biosensing and bioimaging (1-7). For example, the extended photostability and high brightness of QDs are beneficial to single-molecule tracking applications, while the "blinking" nature of QDs improve the localization accuracy for super-resolution techniques such as stochastic optical reconstruction microscopy (7-10). Yet, despite the potential for QDs to improve the current limits of biophysical measurements, their adoption in biomedical investigations is limited. A key limitation of the adoption of QDs arises from concerns regarding steric hinderances due to the large size of QDs compared to traditional fluorophores, as shown in Figure 1. This ultimately necessitates additional control experiments to assess that QD-conjugated targets function similarly to their endogenous and small fluorophore-labeled counterparts (11, 12).

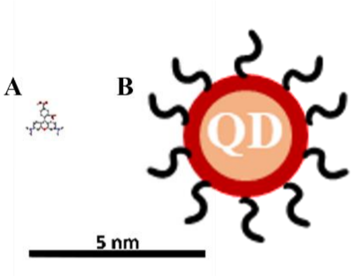

Figure 1. Size comparison of a (A) conventional fluorophore carboxy-tetramethylrhodamine (TAMRA) to a (B) core-shell quantum dot.

However, rather than see the larger size of QDs as a detriment, our work is interested in capitalizing on this feature to construct fluorescent biomimetic structures of biological macromolecules, Specifically, in this study we construct of QD-based biomimetic of SARS-CoV-2 for application in future investigations of COVID-19 associated neuropathophysiology. While QDs have previously been applied in studies of viral activity, such as viral trafficking, the nanoparticles were only applied as a fluorescent marker with no direct biological function (13-16). In the work presented here, we aim to develop a SARS-CoV-2 mimicking QD construct (COVID-QD) that is a high fidelity functional and structural proxy for native SARS-CoV-2 virions. We grow CdSe/CdS core-shell quantum dots via a hot-injection protocol and prepare them for dispersion in biological media via encapsulation in polyethylene glycol (PEG) based polymeric lipid micelle. The hydrophilic end of the phospholipid-PEG ligands are

Colloidal Nanoparticles for Biomedical Applications XVII, edited by Marek Osiński, Antonios G. Kanaras,
Proc. of SPIE Vol. 11977, 1197702 · © 2022 SPIE · 1605-7422 · doi: 10.1117/12.2609118

Downloaded From: https://www.spiedigitallibrary.org/conference-proceedings-of-spie on 17 Apr 2022
Terms of Use: https://www.spiedigitallibrary.org/terms-of-use

terminated with bis(4-methylphenyl)sulfone groups that conjugate individual spike proteins of SARS-CoV-2 via a bisalkylation mechanism at consecutive histidine residues (17). We characterize successful construction of the COVID-QDs via dynamic light scattering (DLS) and photoluminescence (PL) measurements to assess size mimicry and retention of fluorescence properties, respectively. Preliminary data of in-vitro cell cultures treated with the COVID-QDs suggest that our construct is a viable candidate to serve as a proxy to native SARS-CoV-2 to elucidate key viral interactions involved in COVID-19 associated neurological dysfunction.

2. EXPERIMENTAL METHODS

2.1 Synthesis of CdSe/CdS core-shell QDs

The QDs were synthesized following a previously described protocol adapted from Kress *et al.* (7, 18, 19). Briefly, CdSe cores were synthesized by first adding 820 mg CdO, 16.2 g trioctylphosphine oxide (TOPO), 37 g hexadecylamine (HDA), and 3.2 g n-dodecylphosphonic acid (DDPA) to three-neck flask and was heated to 90°C under N_2 and evacuated three times to degas the system. Under N_2 atmosphere, the flask was then heated to 320°C with rapid stirring, until the solution turned clear, and then cooled to 260°C. 8.0 mL of TOP:Se was rapidly injected while stirring and the CdSe cores were grown to the desired size. The reaction was quenched by rapidly cooling to 100°C, followed by injection of 40 mL butanol and cooling to room temperature. The CdSe cores were washed multiple times and then purified via two rounds of size-selective precipitation. The resultant cores were filtered through a 0.45μm syringe filter.

To shell the CdSe cores, 3 mL of oleylamine, 3 mL of octadecene, and 2.2 mL of the CdSe core stock solution were stirred in a three-neck flask and degassed at room temperature to remove the hexanes. The flask was then heated to 115°C, degassed, and then placed under N_2 atmosphere. The Cd (2.26mL of Cd-oleate) and S (0.04mL of octanethiol) precursors were then separately diluted to 3.5mL with octadecene and loaded into separate 5 mL syringe. The syringes were affixed to a syringe pump and precursor injection at a ramp rate of 1.5mL/hr was intiated at 200°C and the flask was heated to 305°C at 16°C/min. The reaction was maintained for two hours at 305°C for shell growth. Then, the flask was cooled to 200°C, 1 mL oleic acid was added dropwise, annealed for one hour, and then cooled to 75°C. The CdSe/CdS core-shell QDs were then washed over three cycles and stored in a glovebox until further use.

2.2 Synthesis of DSPE-PEG$_{2000}$-bis-sulfone

The phospholipid-PEG bisalkylation ligand (PE:PEG:bis-sulfone) was constructed by appending bis(4-methylphenyl)sulfone to phosphatidyethanolamine-PEG (PE:PEG) via a modified NHS-ester crosslinker conjugation adapted from Zhang *et al*. (20). Specifically, DSPE-PEG$_{2k}$-NH$_2$ (Nanocs Inc.) and bis(4-methylphenyl)sulfone-NHS-ester were added to a two-neck flask at a 1:1 mole ratio and degassed under vacuum. The flask was then brought under N_2 atmosphere and a solution of dried dichloromethane containing a 25x excess of triethylamine was injected dropwise to the flask. The reaction volume was kept under N_2 atmosphere and stirred for 48hrs. Aliquots were removed to monitor the reaction progress via thin-layer chromatography with 7.5% methanol:chloroform as the eluting solvent and visualized under short- and long-wave UV irradiation. The reaction mixture was then dried using a rotary evaporator and dissolved with a small volume of dimethylsulfoxide (DMSO) and then diluted with H_2O to a final concentration of <5% DMSO. Unreacted starting material was eluted from the solution using a size-exclusion spin column with a molecular weight cutoff (MWCO) chosen that best fit the approximate diameter of the linear chains. The retained product of PE:PEG:bis-sulfone was collected, freeze dried, and stored a cool, dry environment until further use.

2.3 Construction of COVID-QDs

The CdSe/CdS core-shell quantum dots were then encapsulated into micelles formed by PE:PEG:bis-sulfone via a modified thin-film rehydration protocol as previously reported (7, 21-23). Briefly, CdSe/CdS QDs and PE:PEG:bis-sulfone were dissolved in chloroform at a 1:10,000 mole ratio, vortex mixed, and briefly sonicated before dried under a rotary evaporator. The thin film of QD in polymer was then briefly heated in an 80°C bath before being resuspended in ddH_2O, vortex mixed, and gently stirred for 2 hours. Excess PE:PEG:bis-sulfone was eluted via size-selective spin filtration column with an appropriate MWCO and the retained fraction was prepared for conjugation to His-tagged spike protein via a protocol adapted from Cong *et al.* to produce the COVID-QDs in Figure 2 (17). The QD-PE:PEG:bis-sulfone micelles were incubated at 37°C in sodium phosphate buffer with EDTA before adding 10 molar equivalents of His-tagged spike protein dissolved in sodium acetate buffer with hydroquinone. The reaction mixture was stirred at room temp overnight and then purified with a spin filtration column of an appropriate MWCO. The eluted fraction containing unconjugated

Downloaded From: https://www.spiedigitallibrary.org/conference-proceedings-of-spie on 17 Apr 2022
Terms of Use: https://www.spiedigitallibrary.org/terms-of-use

spike protein was concentrated and measured with a Nanodrop Spectrophotometer to approximate the average number of spike proteins conjugated per COVID-QD. The retained fraction containing the COVID-QDs were characterized with DLS and PL measurements and stored at 4°C until further use.

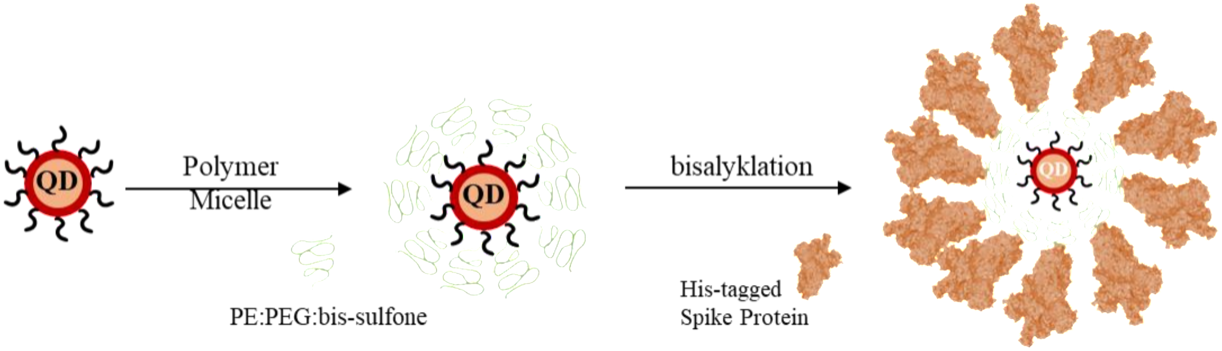

Figure 2. Overview of COVID-QD construction via (1) micelle-encapsulation of CdSe/CdS QDs with PE:PEG:bis-sulfone ligands followed by (2) bisalkylation of His-tagged spike protein to reaction bis-sulfone groups.

2.4 Cell Culture

A model blood-brain barrier, a key component of the NVU, was developed in-vitro by culturing an immortalized murine brain endothelial (bEnd.3) cell line on microporous transwell cell culture inserts. The bEnd.3 cells were seeded at a density of 100,000 cells/well in Dulbecco's Modified Eagle Medium (DMEM) with 10% fetal bovine serum (FBS). The DMEM+10%FBS medium was changed every 2-3 days until cells reached confluency on the inserts and then were treated overnight with either 10nM spike protein or COVID-QDs in DMEM+1%FBS. The treatment was removed and the cultured monolayers were fixed with 4% paraformaldehyde, permeabilized with a solution of 0.25% TritonX-100, blocked with 10% bovine serum albumin, and labeled with a standard indirect immunofluorescent protocol. The membranes were removed from the inserts and mounted onto coverslips and imaged on an Olympus BX51 microscope with appropriate pairs of excitation and emission filters for each channel.

3. RESULTS AND DISCUSSION

3.1 Characterization of COVID-QDs

From the eluted fractions of unconjugated spike protein, we measured an estimated absorbance at 280nm using a NanoDrop spectrophotometer and corrected the absorbance with an estimated extinction coefficient for the spike protein based on the number of tryptophan, phenylalanine, tyrosine, and cysteine residues. Based on this, we estimate that approximately an average of seven spike proteins are conjugated per COVID-QD. While previous structural investigations of SARS-CoV and SARS-CoV-2 virions estimate up to 40 spike proteins may be randomly expressed throughout the virion surface, we believe that the current conjugation efficiency is sufficient for future preliminary investigations in biological cultures (24).

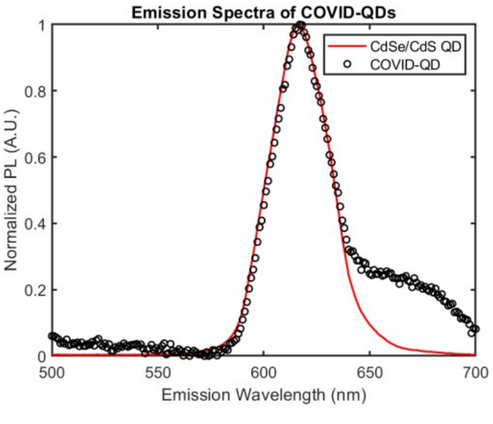

Figure 3. Photoluminescence spectra of CdSe/CdS QDs before and after construction of COVID-QDs.

PL spectra of the retained fraction of "pure" COVID-QDs was measured and compared to the PL spectra of the CdSe/CdS QDs prior to micellation and conjugation, as shown in Figure 3. From the normalized PL spectra, it is observed that the peak emission wavelength does not shift, though an inhomogeneous broadening is observed likely resultant from small QD aggregates forming in some of the larger COVID-QD micelles. The potential for the formation of such QD aggregates in some COVID-QD constructs and not others is verified by a preliminary DLS distribution plot acquired on a Wyatt DLS instrument (Figure 4). While the distribution exhibits the presence of COVID-QDs within the full estimated range of SARS-CoV-2 virion sizes (~60nm to ~140nm), the average hydrodynamic radius ($\bar{R}_H$) as computed by a %Number normalization reports a size of 77.9nm

Downloaded From: https://www.spiedigitallibrary.org/conference-proceedings-of-spie on 17 Apr 2022
Terms of Use: https://www.spiedigitallibrary.org/terms-of-use

for the COVID-QD constructs (25-27). This is on the upper limit of this range and may lead to potential artifacts in future biological studies, where the larger COVID-QDs may not be high fidelity proxies for the steric hinderances a native SARS-CoV-2 virion may encounter. Potential mechanisms to address this may include additional size-selection filtration as well as optimization studies of QD loading into micelles to isolate more monodisperse size distributions. Another potential option may be to alter the PEG chain length of PE:PEG:bis-sulfone, and is of interest in our future studies. Nevertheless, the data shown here are indicative that our protocol can produce high fidelity structural mimics of SARS-CoV-2 that retain the intrinsic enhanced photophysical properties of QDs.

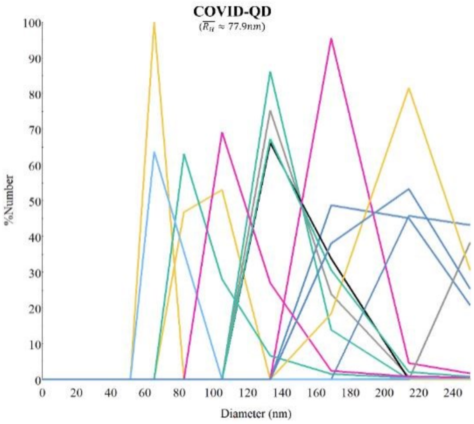

Figure 4. DLS distribution of COVID-QD constructs, where each peak represents the %Number diameter for a replicate sample.

3.2 COVID-QD treated cultures of bEnd.3 monolayers

To assess for the functional mimicry of our COVID-QD constructs, we treated monolayers of bEnd.3 cells cultured on transwell cell culture inserts with equimolar treatments of either 10nM spike protein of 10nM COVID-QDs. The concentration of the COVID-QD treatment is based on an estimated concentration of QDs incorporated into COVID-QDs. The monolayers were than stained with an indirect immunofluorescent labeling protocol to examine changes in the expression of platelet endothelial adhesion molecule 1 (PECAM-1) and a tight juction protein claudin-5 (CLDN-5) and shown in Figure 5. From these immunofluorescent images, it is clear that the observed fluorescence from the QD emission channel (633nm LPF) is unique to the COVID-QD treatment group, indicating that the construct has a target on the cells. The binding of the COVID-QDs to the cells is additionally confirmed by the localization of QD emission within the cellular borders traced by PECAM-1 and centered around the nuclei. In terms of actual functional mimicry, we observe similar dysregulation of the localization of the CLDN-5 in both the COVID-QD and spike protein treated groups. The tight junction protein CLDN-5 is observed to exhibit less colocalization with PECAM-1, indicating disruption of paracellular gaps in the barrier. This observation is of interest for consideration as to how pathogenic challenge by SARS-CoV-2 may induce immunomodulatory events in the central nervous system. Disruption of the paracellular gaps of the blood-brain barrier may lead to increased leakage into the central nervous system, leading to aberrant neuroinflammation that may be associated with the neurological deficits observed in COVID-19 pathogenesis. In our future work, we hope to further explore modulation of the NVU in response to our COVID-QDs and examine whether targets exist within the central nervous system for COVID-QDs, and by proxy SARS-CoV-2, to mediate direct immunomodulation.

4. CONCLUSIONS

From the data presented here, we have constructed a functional and structural biomimetic of SARS-CoV-2 from CdSe/CdS core-shell QDs. By encapsulating the QDs in micelles formed by PE:PEG:bis-sulfone, multiple his-tagged spike proteins were conjugated per COVID-QD via a bisalyklation mechanism. The overall size distribution of the COVID-QDs fall within the estimated range of SARS-CoV-2 virions, and preliminary investigations with a model blood-brain barrier culture indicate similar functional effects between COVID-QDs and soluble spike protein. The ability to use a noninfectious and fluorescent proxy of SARS-CoV-2 in cultured model systems for the NVU will be useful to better elucidate the mechanisms leading to the neurological deficits observed in COVID-19 infection and post-acute sequelae. In our future work, we hope to optimize the conjugation efficiency and size distribution of the COVID-QD constructs and apply them to more complex co-culture systems of the NVU.

5. ACKNOWLEDGEMENTS

We would like to acknowledge the NSF (CHE-1904847) and NIH (T32GM135134, R01AG057525) for supporting various portions of this work.

Downloaded From: https://www.spiedigitallibrary.org/conference-proceedings-of-spie on 17 Apr 2022
Terms of Use: https://www.spiedigitallibrary.org/terms-of-use

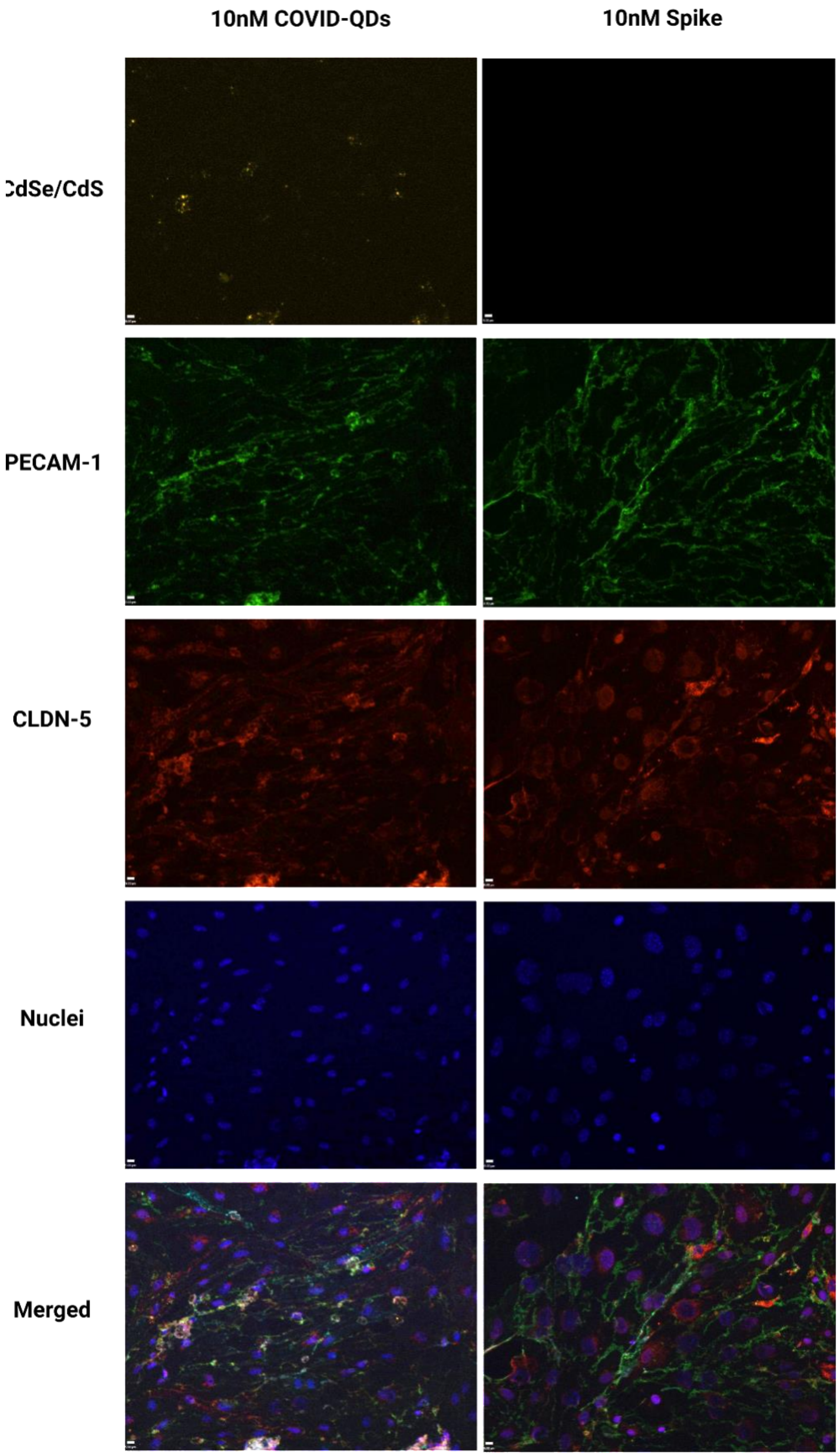

Figure 5. Immunofluorescent images taken of bEnd.3 monolayers cultured on transwell inserts and treated with either 10nM COVID-QDs or 10nM soluble spike protein. The excitation and emission pairs for the various channels are as follows: QD ($\lambda_{ex} = 350nm$, 633nm LPF), PECAM-1 ($\lambda_{ex} = 488nm$, 510nm BPF), CLDN-5 ($\lambda_{ex} = 568nm$, 610nm BPF), Nuclei ($\lambda_{ex} = 350nm$, 420nm BPF).

Downloaded From: https://www.spiedigitallibrary.org/conference-proceedings-of-spie on 17 Apr 2022
Terms of Use: https://www.spiedigitallibrary.org/terms-of-use

6. REFERENCES

1. Bilan R, Nabiev I, Sukhanova A. Quantum Dot-Based Nanotools for Bioimaging, Diagnostics, and Drug Delivery. *Chembiochem*. 2016;17(22):2103-14. Epub 2016/08/19. doi: 10.1002/cbic.201600357. PubMed PMID: 27535363.
2. Cai E, Ge P, Lee SH, Jeyifous O, Wang Y, Liu Y, et al. Stable small quantum dots for synaptic receptor tracking on live neurons. *Angew Chem Int Ed Engl*. 2014;53(46):12484-8. Epub 2014/09/27. doi: 10.1002/anie.201405735. PubMed PMID: 25255882; PMCID: PMC4240739.
3. Dai W-X, Zhang L, Zhao W-W, Yu X-D, Xu J-J, Chen H-Y. Hybrid PbS Quantum Dot/Nanoporous NiO Film Nanostructure: Preparation, Characterization, and Application for a Self-Powered Cathodic Photoelectrochemical Biosensor. *Analytical Chemistry*. 2017;89(15):8070-8. doi: 10.1021/acs.analchem.7b01557.
4. Geißler D, Charbonnière LJ, Ziessel RF, Butlin NG, Löhmannsröben H-G, Hildebrandt N. Quantum Dot Biosensors for Ultrasensitive Multiplexed Diagnostics. *Angewandte Chemie International Edition*. 2010;49(8):1396-401. doi: 10.1002/anie.200906399.
5. Gorshkov K, Susumu K, Chen J, Xu M, Pradhan M, Zhu W, et al. Quantum Dot-Conjugated SARS-CoV-2 Spike Pseudo-Virions Enable Tracking of Angiotensin Converting Enzyme 2 Binding and Endocytosis. *ACS Nano*. 2020;14(9):12234-47. doi: 10.1021/acsnano.0c05975; PMCID: PMC7482579.
6. Liu Y, Oda H, Inoue Y, Ishihara K. Movement of a Quantum Dot Covered with Cytocompatible and pH-Responsible Phospholipid Polymer Chains under a Cellular Environment. *Biomacromolecules*. 2016;17(12):3986-94. Epub 2016/10/30. doi: 10.1021/acs.biomac.6b01357. PubMed PMID: 27791358.
7. Urban JM, Chiang W, Hammond JW, Cogan NMB, Litzburg A, Burke R, et al. Quantum Dots for Improved Single-Molecule Localization Microscopy. *The Journal of Physical Chemistry B*. 2021;125(10):2566-76. doi: 10.1021/acs.jpcb.0c11545; PMCID: PMC8080873.
8. Wichner SM, Mann VR, Powers AS, Segal MA, Mir M, Bandaria JN, et al. Covalent Protein Labeling and Improved Single-Molecule Optical Properties of Aqueous CdSe/CdS Quantum Dots. *ACS Nano*. 2017;11(7):6773-81. doi: 10.1021/acsnano.7b01470; PMCID: PMC5891212.
9. Yang X, Zhanghao K, Wang H, Liu Y, Wang F, Zhang X, et al. Versatile Application of Fluorescent Quantum Dot Labels in Super-resolution Fluorescence Microscopy. *ACS Photonics*. 2016;3(9):1611-8. doi: 10.1021/acsphotonics.6b00178.
10. Thal LB, Mann VR, Sprinzen D, McBride JR, Reid KR, Tomlinson ID, et al. Ligand-conjugated quantum dots for fast sub-diffraction protein tracking in acute brain slices. *Biomaterials Science*. 2020;8(3):837-45. doi: 10.1039/c9bm01629e; PMCID: PMC7002256.
11. Vu TQ, Lam WY, Hatch EW, Lidke DS. Quantum dots for quantitative imaging: from single molecules to tissue. *Cell and Tissue Research*. 2015;360(1):71-86. doi: 10.1007/s00441-014-2087-2.
12. Resch-Genger U, Grabolle M, Cavaliere-Jaricot S, Nitschke R, Nann T. Quantum dots versus organic dyes as fluorescent labels. *Nature Methods*. 2008;5(9):763-75. doi: 10.1038/nmeth.1248.
13. Qin C, Li W, Li Q, Yin W, Zhang X, Zhang Z, et al. Real-time dissection of dynamic uncoating of individual influenza viruses. *Proceedings of the National Academy of Sciences*. 2019;116(7):2577-82. doi: 10.1073/pnas.1812632116; PMCID: PMC6377448.
14. Wen L, Zheng Z-H, Liu A-A, Lv C, Zhang L-J, Ao J, et al. Tracking single baculovirus retrograde transportation in host cell via quantum dot-labeling of virus internal component. *Journal of Nanobiotechnology*. 2017;15(1). doi: 10.1186/s12951-017-0270-9; PMCID: PMC5420409.
15. Yang YB, Tang YD, Hu Y, Yu F, Xiong JY, Sun MX, et al. Single Virus Tracking with Quantum Dots Packaged into Enveloped Viruses Using CRISPR. *Nano Lett*. 2020;20(2):1417-27. Epub 2020/01/14. doi: 10.1021/acs.nanolett.9b05103. PubMed PMID: 31930919.
16. Dixit SK, Goicochea NL, Daniel M-C, Murali A, Bronstein L, De M, et al. Quantum Dot Encapsulation in Viral Capsids. *Nano Letters*. 2006;6(9):1993-9. doi: 10.1021/nl061165u.
17. Cong Y, Pawlisz E, Bryant P, Balan S, Laurine E, Tommasi R, et al. Site-Specific PEGylation at Histidine Tags. *Bioconjugate Chemistry*. 2012;23(2):248-63. doi: 10.1021/bc200530x.
18. Kress SJ, Richner P, Jayanti SV, Galliker P, Kim DK, Poulikakos D, et al. Near-field light design with colloidal quantum dots for photonics and plasmonics. *Nano Lett*. 2014;14(10):5827-33. Epub 2014/09/03. doi: 10.1021/nl5026997. PubMed PMID: 25180812.

Downloaded From: https://www.spiedigitallibrary.org/conference-proceedings-of-spie on 17 Apr 2022
Terms of Use: https://www.spiedigitallibrary.org/terms-of-use

19. Kress SJ, Antolinez FV, Richner P, Jayanti SV, Kim DK, Prins F, et al. Wedge Waveguides and Resonators for Quantum Plasmonics. *Nano Lett*. 2015;15(9):6267-75. Epub 2015/08/19. doi: 10.1021/acs.nanolett.5b03051. PubMed PMID: 26284499; PMCID: PMC4566130.
20. Zhang H, Weingart J, Jiang R, Peng J, Wu Q, Sun XL. Bio-inspired liposomal thrombomodulin conjugate through bio-orthogonal chemistry. *Bioconjug Chem*. 2013;24(4):550-9. Epub 2013/03/06. doi: 10.1021/bc300399f. PubMed PMID: 23458546; PMCID: PMC3630279.
21. Carion O, Mahler B, Pons T, Dubertret B. Synthesis, encapsulation, purification and coupling of single quantum dots in phospholipid micelles for their use in cellular and in vivo imaging. *Nature Protocols*. 2007;2(10):2383-90. doi: 10.1038/nprot.2007.351.
22. Maiseyeu A, Bagalkot V. In vitro uptake of apoptotic body mimicking phosphatidylserine-quantum dot micelles by monocytic cell line. *Nanoscale Res Lett*. 2014;9(1):176. Epub 2014/04/15. doi: 10.1186/1556-276X-9-176. PubMed PMID: 24725273; PMCID: PMC4022335.
23. Fan H, Leve EW, Scullin C, Gabaldon J, Tallant D, Bunge S, et al. Surfactant-Assisted Synthesis of Water-Soluble and Biocompatible Semiconductor Quantum Dot Micelles. *Nano Letters*. 2005;5(4):645-8. doi: 10.1021/nl050017l.
24. Turoňová B, Sikora M, Schürmann C, Hagen WJH, Welsch S, Blanc FEC, et al. In situ structural analysis of SARS-CoV-2 spike reveals flexibility mediated by three hinges. *Science*. 2020;370(6513):203-8. doi: 10.1126/science.abd5223; PMCID: PMC7665311.
25. Li F. Structure, Function, and Evolution of Coronavirus Spike Proteins. *Annu Rev Virol*. 2016;3(1):237-61. Epub 2016/09/01. doi: 10.1146/annurev-virology-110615-042301. PubMed PMID: 27578435; PMCID: PMC5457962.
26. Beniac DR, Andonov A, Grudeski E, Booth TF. Architecture of the SARS coronavirus prefusion spike. *Nature Structural & Molecular Biology*. 2006;13(8):751-2. doi: 10.1038/nsmb1123; PMCID: PMC7097490.
27. Varga Z, Flammer AJ, Steiger P, Haberecker M, Andermatt R, Zinkernagel A, et al. Electron microscopy of SARS-CoV-2: a challenging task – Authors' reply. *The Lancet*. 2020;395(10238):e100. doi: 10.1016/s0140-6736(20)31185-5; PMCID: PMC7237177.

Downloaded From: https://www.spiedigitallibrary.org/conference-proceedings-of-spie on 17 Apr 2022
Terms of Use: https://www.spiedigitallibrary.org/terms-of-use